Supplemental material Table of Contents

Supplemental Methods

- **Measurement of renal function**
- **Histological evaluation**
- **Western blotting**
- **Quantitative Real-time PCR**
- **Immunohistochemistry/Immunofluorescence**
- **In situ hybridization**
- **TUNEL assay**
- **Co-immunoprecipitation**

Supplemental Tables

- **Supplemental Table 1. PCR reaction and products used for the genotyping of the triple transgenic Pax8-rtTA/LC1-Cre/Tet-o-Periostin mice.**
- **Supplemental Table 2. Primer sequences used for quantitative Real-time PCR.**

Supplemental Figure legends

- **Supplemental Figure 1. Co-localization of periostin with different renal tubular markers in WT mice 72h after I/R.**
- **Supplemental Figure 2. Kidney/body weight ratio of periostin-overexpressing and KO mice compared to their respective controls at basal conditions and 72h after I/R.**
- **Supplemental Figure 3. Periostin protects from apoptosis induction after I/R.**
- **Supplemental Figure 4. Periostin promotes proliferation of tubular cells after I/R.**
- **Supplemental Figure 5. Periostin inhibits the activation of the Itgβ1 downstream targets FAK and ERK.**
- **Supplemental Figure 6. Periostin protects primary tubular cells from oxidative stress-induced cell death.**
- **Supplemental Figure 7. Recombinant periostin directly promotes the polarization and proliferation of cultured macrophages.**
- **Supplemental Figure 8. Chronic periostin overexpression is not linked to a profibrotic phenotype.**
- **Supplemental Figure 9. Periostin protects from fibrosis development 6w after I/R.**
- **Supplemental Figure 10. M2a markers are not increased in renal macrophages derived from periostin-overexpressing mice.**

Supplemental Figures

Supplemental Methods

Measurement of renal function

Blood urea and creatinine levels were measured with an enzymatic method (Konelab analyzer) and expressed in millimoles per liter and micromoles per liter respectively.

Histological evaluation

Formalin-fixed, paraffin-embedded, 4-µm thick kidney sections were stained with Periodic Acid-Schiff (PAS) or Sirius Red. Quantifications were performed by examining at least 10 microphotographs of random, non-overlapping fields at 200x magnification per mouse. Tubular dilation and necrosis were evaluated semi-quantitatively in PAS-stained slides, using the following scale: 0, no tubular damage; 1, damage in 1–25% of the tubules analyzed; 2, damage in 26–50% of the tubules analyzed; 3, damage in 51–75% of the tubules analyzed; 4, damage in >76% of the tubules analyzed, and the mean value was calculated for each mouse. Tubular injury was evaluated as simultaneous quantification of both tubular dilation and necrosis. Interstitial fibrosis was evaluated by quantifying the Sirius Red-positive area, excluding glomeruli and large vessels, using the Image J Fiji software.

Western blotting

Proteins from quarter kidneys or cell cultures were extracted in a commercial RIPA lysis buffer supplemented with PMSF, a protease inhibitor cocktail and sodium orthovanadate (Santa Cruz) and total protein concentration was measured using the Bradford assay. Equal amounts of proteins were loaded on a NuPAGE 4-12% gradient gel (Invitrogen) and transferred to nitrocellulose membrane (Biorad). Immunoblotting was performed for periostin (R&D Systems, MAB3548), integrin-β1 (Abcam, ab183666), p-JNK (Cell Signaling #9251), JNK (Cell Signaling #9252), p-AKT Ser473 (Cell Signaling #9271), AKT (Santa Cruz, sc-8312), p-FAK Y576 (Abcam, ab76120), FAK (Santa Cruz, sc-557), p-ERK (Santa Cruz, sc-16982), ERK 2 (Santa Cruz, sc-154), Bax (Cell Signaling #27725), p53 (Santa Cruz, sc-6243), p21 (Abcam, ab188224), p-CDK1 (p-CDC2) Tyr15 (Cell Signaling #9111), CD163 (Novus Biologicals, NBP2-36494SS), LIF (R&D Systems, MAB449), uPA (R&D Systems, MAB9185). Gapdh (Sigma, G9545) or β-actin (Novus Biologicals, NB100-56874) was used as loading control.

Quantitative Real-time PCR

Total RNA was extracted from quarter kidneys using TRI Reagent (MRC) and from cell cultures using the EZ-10 Spin Column Total RNA Mini-preps Super kit (Bio Basic Inc). RNA quality was verified by measuring the OD 260/280 ratio and residual genomic DNA was removed by DNase I treatment (Thermo Scientific) for 30 minutes at 37°C. 1µg RNA was transcribed to cDNA using the Maxima First Strand cDNA Synthesis Kit from Thermo Scientific according to manufacturer's instructions. Real-time PCR was performed with the Roche Light Cycler 480® detection system using SYBR Green PCR Master Mix (Roche). Specific primers for target mRNAs (Supplemental Table 2) were used for amplification under

the following program: 95°C for 5 minutes, 45 cycles at 95°C for 15 seconds, 60°C for 15 seconds and 72°C for 15 seconds. For quantitative analysis, experimental genes were normalized to *Hprt* or *Rpl32* mRNA expression using the ΔΔCT method. Dissociation curves were analyzed in order to determine that a single product was amplified.

Immunohistochemistry/Immunofluorescence

For immunostaining of macrophages, 4-µm formalin-fixed, paraffin-embedded kidney sections were stained with primary antibodies to F4/80 (Abd Serotec MCA497R) or CD68 (Abcam ab125212). Appropriate secondary antibodies (N-Histofine, Nichirei Biosciences) and AEC (Dako) as substrate were used. Slides were counterstained with hematoxylin QS (Vector) and mounted with permanent aqueous mounting medium (ScyTek). The F4/80 or CD68 positive area was quantified in at least 10 photographs at 200x magnification per animal, using publicly available image processing software (Image J Fiji), and expressed as percentage of the total tissue area.

For periostin immunostaining, 5-µm frozen tissue sections were fixed in acetone, blocked and permeabilized in 10% FBS-0.1% Triton X-100 and incubated with primary anti-periostin (R&D Systems, MAB3548) antibody. For integrin-β1 (Abcam ab183666) and KIM-1 (Abcam ab47635) immunostaining, 4-µm formalin-fixed, paraffin-embedded kidney sections were used. Incubation with secondary antibodies and signal detection was performed as described above. KIM-1 positive area was quantified in at least 10 photographs at 200x magnification per animal and expressed as percentage of total tissue area.

Single or double immunofluorescence labeling was performed on 4-µm paraffin tissue sections, 5-µm frozen tissue sections or cells seeded on coverslips. The sections were rehydrated and the cells were fixed in 10% PFA, followed by blocking/permeabilization in 10% FBS-0.1% Triton X-100 and incubation with primary antibodies to periostin (R&D Systems, MAB3548), integrin-β1 (Abcam ab183666), F4/80 (Abd Serotec MCA497R), MCM2 (Cell Signaling #4007), CD206 (Bio-rad MCA2235GA), PCNA (Cell Signaling #13110), p-H3 (Cell Signaling #9701), cleaved caspase-3 (Cell Signaling #D175), collagen I (Abcam ab21286), aquaporin-1 (Abcam ab9566), Na+-Cl− cotransporter (NCC, MRC PPU Dundee), Na-K-Cl 2 cotransporter (NKCC2, MRC PPU Dundee) or DBA lectin (Vector RL-1032). The signal was detected with Alexa Fluor secondary antibodies followed by DAPI counterstain and mounting in PermaFluor medium (Thermo Scientific). $MCM2^+$ and $PCNA^+$ F4/80 macrophages were quantified in at least 10 photographs at 200x-400x magnification per animal and expressed as number of positive macrophages per high power field. Cleaved caspase 3 was quantified in 8-10 photographs at 200x-400x magnification per sample and expressed as mean number of positive cells (in vitro) or positive tubules (in vivo) per field (a positive tubule was defined as a tubule with at least one cell positive). p-H3 staining was quantified in 10 photographs at 200x magnification per sample and expressed as percentage of p-H3-positive cells to dapi.

In situ hybridization

The RNAscope 2.0 HD Detection Kit-Brown and a mouse periostin specific probe (Advanced Cell Diagnostics) were used according to manufacturer's instructions. Briefly, 5-μm frozen tissue sections were fixed in 4% PFA for 15 min, dehydrated through increasing concentrations of EtOH, dried at room temperature, treated with peroxidase blocking and proteinase solutions and hybridized with the mouse periostin probe, as well as a positive and a negative control probe at 40^{o}C for 2 hours. This was followed by signal amplification hybridization steps at 40^{o}C or room temperature before detection of the signal with a DAB chromogen. The slides were counterstained with hematoxylin, dehydrated and mounted.

TUNEL assay

Apoptosis was evaluated with the DeadEnd^{TM} Fluorometric TUNEL System (Promega) according to manufacturer's instructions on 4-μm paraffin sections. Quantifications were performed by examining at least 10 microphotographs of random, non-overlapping fields at 200x-400x magnification per mouse. The results were expressed as number of TUNEL positive nuclei per high power field.

Co-immunoprecipitation

Protein interactions were stabilized by crosslinking minced quarter kidneys with DTSSP (Thermo Scientific #21578) according to manufacturer's instructions. Proteins were extracted in Pierce IP lysis buffer (#87787) supplemented with PMSF, a protease inhibitor cocktail and sodium orthovanadate and total protein concentration was measured using the Bradford assay. Equal amounts of proteins were precipitated with a rabbit anti-integrin-β1 antibody (Abcam ab183666) and rabbit IgG was used as control. The precipitated complexes were purified with the use of Protein G Magnetic Beads (Cell Signaling #8740) and loaded on a denaturing SDS-PAGE followed by Western Blot. Equal amounts of Input were also loaded on the same gel. Immunoblotting was performed for periostin (R&D Systems, MOSF20) and the membrane was stripped using RestoreTM Western Blot Stripping Buffer (Thermo Scientific #21059) and re-blotted for integrin-β1 (Abcam ab183666). Veriblot for IP secondary antibody (Abcam ab131366) detecting preferentially the non-reduced form of the IgG was used, in order to avoid non-specific signal from co-eluted reduced forms of the antibodies used for IP.

Supplemental Tables

Supplemental Table 1. PCR reaction and products used for the genotyping of the triple transgenic Pax8-rtTA/LC1-Cre/Tet-o-Periostin mice.

PCR products				**PCR reaction**	
Gene	**Primer**	**Sequence 5'-3'**	**Product length (bp)**	**Temperature (°C)**	**Time (min)**
Pax8	Sense	CCATGTCTAGACTGGACAAGA	550	95	1
	Antisense	CTCCAGGCCACATATGATTAG		95	1
LC1	Sense	TCGCTGCATTACCGGTCGATGC	400	55	1
	Antisense	CCATGAGTGAACGAACCTGGTCG		72	1
Tet-o-Periostin	Sense	GATTGGGAAGACAATAGCAGGCATG	350	Go to step 2 39 times	
	Antisense	TCTTCCCGCAGATAGCACCTTG		72	10
				4	forever

Supplemental Table 2. Primer sequences used for quantitative Real-time PCR.

Gene	**Primer**	**Sequence 5'-3'**
Periostin	Sense	CGGGAAGAACGAATCATTACA
	Antisense	ACCTTGGAGACCTCTTTTTGC
Ngal	Sense	CCATCTATGAGCTACAAGAGAACAAT
	Antisense	TCTGATCCAGTAGCGACAGC
Kim-1	Sense	TCAGATTCAAGTCTTCATTTCAGG
	Antisense	CCCCCTTTACTTCCACATAAGAA
Il-6	Sense	GCTACCAAACTGGATATAATCAGGA
	Antisense	CCAGGTAGCTATGGTACTCCAGAA
Mcp-1	Sense	GGCTGGAGAGCTACAAGAGG
	Antisense	CTCTTGAGCTTGGTGACAAAAA
Vcam-1	Sense	TCTTACCTGTGCGCTGTGAC
	Antisense	ACTGGATCTTCAGGGAATGAGT
Cdkn1a	Sense	AACATCTCAGGGCCGAAA
	Antisense	TGCGCTTGGAGTGATAGAAA
Ckdn2a	Sense	GGGTTTTCTTGGTGAAGTTCG
	Antisense	TTGCCCATCATCATCACCT
Cd163	Sense	TCTCAGTGCCTCTGCTGTCA
	Antisense	CGCCAGTCTCAGTTCCTTCT
Il-10	Sense	ACTGCACCCACTTCCCAGT
	Antisense	TGTCCAGCTGGTCCTTTGTT
Csf-1	Sense	CAGCTGCTTCACCAAGGACT
	Antisense	TCATGGAAAGTTCGGACACA
uPA	Sense	GGAGCAGCTCATCTTGCAC

	Antisense	CCCGTGCTGGTACGTATCTT
Lif	Sense	AAACGGCCTGCATCTAAGG
	Antisense	AGCAGCAGTAAGGGCACAAT
Hb-egf	Sense	TCTTGTCATCGTGGGACTTCT
	Antisense	CACGCCCAACTTCACTTTCT
Cd206	Sense	CCACAGCATTGAGGAGTTTG
	Antisense	ACAGCTCATCATTTGGCTCA
Arg1	Sense	CCTGAAGGAACTGAAAGGAAAG
	Antisense	TTGGCAGATATGCAGGGAGT
Ym1	Sense	AAGAACACTGAGCTAAAAACTCTCCT
	Antisense	GAGACCATGGCACTGAACG
Col1a1	Sense	CATGTTCAGCTTTGTGGACCT
	Antisense	GCAGCTGACTTCAGGGATGT
Col3a1	Sense	TGGTTTCTTCTCACCCTTCTTC
	Antisense	TGCATCCCAATTCATCTACGT
Fibronectin	Sense	CGGAGAGAGTGCCCCTACTA
	Antisense	CGATATTGGTGAATCGCAGA
Hprt	Sense	GGAGCGGTAGCACCTCCT
	Antisense	CTGGTTCATCATCGCTAATCAC
Rpl32	Sense	GCTGCCATCTGTTTTACGG
	Antisense	TGACTGGTGCCTGATGAACT

Supplemental Figure legends

Supplemental Figure 1

Co-localization of periostin with different renal tubular markers in WT mice 72h after I/R. (A) A broad expression of periostin is observed around injured proximal tubular cells (marked with acquaporin-1). (B) There is a little expression of periostin (arrows) around cortical distal tubular cells, marked by Na^+-Cl^- cotransporter (NCC). (C) A broad expression of periostin is evident around Na-K-Cl-2 cotransporter (NKCC2)-positive tubules, marking the thick ascending limb of the loop of Henle. (D) Periostin is expressed around a subset of collecting duct tubular cells, marked by Dolichos Biflorus Agglutinin (DBA) lectin. Representative images are shown. Scale bars: 100 µm (left image), 50 µm (right image, magnification of the white frame).

Supplemental Figure 2

Kidney/body weight ratio of periostin-overexpressing and KO mice compared to their respective controls at basal conditions and 72h after I/R. (A) Kidney/body weight ratio is not different between control and periostin-overexpressing mice, but increases in both groups after I/R. (B) Kidney/body weight ratio is not different between WT and periostin KO

mice, but increases significantly in KO mice after I/R, with a tendency to increase in WT mice. *P<0.05 vs. CNT, POSTN or KO. n=4-6 mice per group.

Supplemental Figure 3

Periostin protects from apoptosis induction after I/R. (A, B) The induction of cleaved caspase-3 is lower in periostin-overexpressing mice (A) and higher in periostin KO mice (B) compared to control or WT mice, respectively, 24h after I/R. Representative images are shown. Scale bars: 50 μm. $^{\#}P$<0.05 vs. CNT I/R or WT I/R. n=5 mice per group.

Supplemental Figure 4

Periostin promotes proliferation of tubular cells after I/R. (A) FACS analysis showing selection of $PAX8^{+}$ tubular cells (left) and cell cycle analysis of the selected population in control, periostin-overexpressing, WT and periostin KO groups (right). (B) Quantification of the percentage of $PAX8^{+}$ cells from control and periostin-overexpressing mice in different cell cycle phases 72h after I/R, showing decreased proportion of periostin-overexpressing tubular cells in G0G1 phase and increased proportion in S phase. (C) Quantification of the percentage of $PAX8^{+}$ cells from WT and periostin KO mice in different cell cycle phases 72h after I/R, showing increased proportion of KO tubular cells in G0G1 phase and decreased proportion in S and G2M phases. Representative images are shown. $^{\#}P$<0.05, $^{\#\#\#}P$<0.001 vs. CNT I/R 72h or WT I/R 72h. n=4-5 per group.

Supplemental Figure 5

Periostin inhibits the activation of the Itgβ1 downstream targets FAK and ERK. (A) Western blot and quantifications of p-FAK and p-ERK in control and periostin-overexpressing mice 24h after I/R, showing that p-FAK was decreased in both strains, while p-ERK was increased at a lower level in the overexpressing mice after I/R. (B) Western blot and quantifications of p-FAK and p-ERK in WT and periostin KO mice, showing that both p-FAK and p-ERK were significantly increased in KO mice 24h after I/R. *P<0.05, **P<0.01, ***P<0.001 vs. CNT, POSTN or CTL, $^{\#\#}P$<0.01, $^{\#\#\#}P$<0.001 vs. CNT I/R 24h or WT I/R 24h. n=2-3 for CNT or CTL and 4-5 per I/R group.

Supplemental Figure 6

Periostin protects primary tubular cells from oxidative stress-induced cell death. (A) Cleaved caspase 3 (green) is increased 2hr after H_2O_2 treatment in periostin KO compared to WT cells. Co-staining with phalloidin (red) is shown. (B, C) LDH release, indicative of cell death, is higher (B), while cell survival assessed by crystal violet staining, is progressively decreased in KO compared to WT cells (C), after H_2O_2 treatment. (D) Periostin is produced by cultured WT tubular cells and is absent from KO cells, while Itgβ1 is similarly expressed by both cell strains prior and after H_2O_2 treatment. AKT is more highly activated in cells expressing periostin both prior and after H_2O_2 treatment, while p53 is only induced in KO cells after oxidative stress induction. Representative images are shown. Scale bars: 50 μm.

*P<0.05, **P<0.01, ***P<0.001 vs. CTL, $^{\#}P$<0.05, $^{\#\#}P$<0.01, $^{\#\#\#}P$<0.001 vs. WT H_2O_2. Quantifications of 2-3 independent experiments performed in duplicates or triplicates are shown.

Supplemental Figure 7

Recombinant periostin directly promotes the polarization and proliferation of cultured macrophages. (A-F) mRNA expression of different factors in RAW macrophages after treatment with recombinant periostin for 48h. Exogenous periostin induced lower expression of IL-6 (A) and IL-1β (B) and higher expression of IL-10 (C), CD163 (D), uPA (E) and LIF (F) in RAW macrophages. (G) Treatment with recombinant periostin induced higher proliferation in RAW macrophages compared to non-treated cells, assessed by crystal violet staining. ***P<0.001 vs. RAW 0h, $^{\#}P$<0.05, $^{\#\#}P$<0.01 vs. RAW or RAW 48h. Quantifications of 2-3 independent experiments performed in duplicates (A-F) or quadruplicates (G) are shown.

Supplemental Figure 8

Chronic periostin overexpression is not linked to a profibrotic phenotype. (A, B) Col1 (A) and Col3 (B) mRNA expression in control mice and mice overexpressing periostin for 2 and 4 months, showing no significant difference between groups. (C, D) Sirius Red quantification (C) and staining (D) in control mice and mice overexpressing periostin for 2 and 4 months, showing no significant increase of interstitial matrix deposition after chronic periostin overexpression. (E) Western blot and quantification of periostin protein expression after 4 months of chronic overexpression, showing an abundant production of periostin in the kidney. (F-H) mRNA expression of different profibrotic genes in control and periostin-overexpressing mice, 24h and 72h after I/R. Col1 (F), Col3 (G) and fibronectin (H) are less increased in periostin-overexpressing mice 72h after I/R. Representative images are shown. Scale bars: 100 µm. *P<0.05, **P<0.01, ***P<0.001 vs. CNT 72h or POSTN 72h, $^{\#}P$<0.05, $^{\#\#}P$<0.01, $^{\#\#\#}P$<0.001 vs. CNT 4m or CNT I/R 72h. n=3 for CNT 24h or 72h and 4-6 per I/R or chronic overexpression group.

Supplemental Figure 9

Periostin protects from fibrosis development 6w after I/R. (A) Sirius Red staining and quantification in control and periostin-overexpressing mice 6 weeks after I/R, showing decreased interstitial matrix deposition in mice that overexpressed periostin when I/R was performed. (B) Collagen I staining and quantification in control and periostin-overexpressing mice 6 weeks after I/R, showing decreased collagen I accumulation in mice that overexpressed periostin when I/R was performed. (C, D) Sirius Red (C) and collagen I (D) staining and quantifications in WT and periostin KO mice 6 weeks after I/R, showing increased interstitial matrix deposition and collagen I accumulation in KO mice 6 weeks after I/R. (E, F) Western blot and quantification of periostin protein expression in control and periostin-overexpressing mice (E) or WT and periostin KO mice (F) 6 weeks after I/R. Periostin induction is lower in the chronic phase compared to the acute phase of I/R, 24h-

72h (see figure 1). Representative images are shown. Scale bars: 200 µm (A, C), 100 µm (B, D). *P<0.05, **P<0.01 vs. CNT, POSTN or WT CTL, $^{\#}P$<0.05, $^{\#\#}P$<0.01, $^{\#\#\#}P$<0.001 vs. CNT, CNT I/R or WT I/R. n=3 for CNT, POSTN or CTL and 5-6 per I/R group.

Supplemental Figure 10

M2a markers are not increased in renal macrophages derived from periostin-overexpressing mice. (A-C) mRNA expression of different M2a markers in F4/80^{+} macrophages isolated from control and periostin-overexpressing mice 72h after I/R. CD206 levels are similar (A), while expression of the pro-reparative molecules Arg1 (B) and Ym1 (C) is lower in macrophages from periostin-overexpressing mice. $^{\#}P$<0.05 vs. CNT I/R. n=5 mice per group.

Supplemental Figure 1

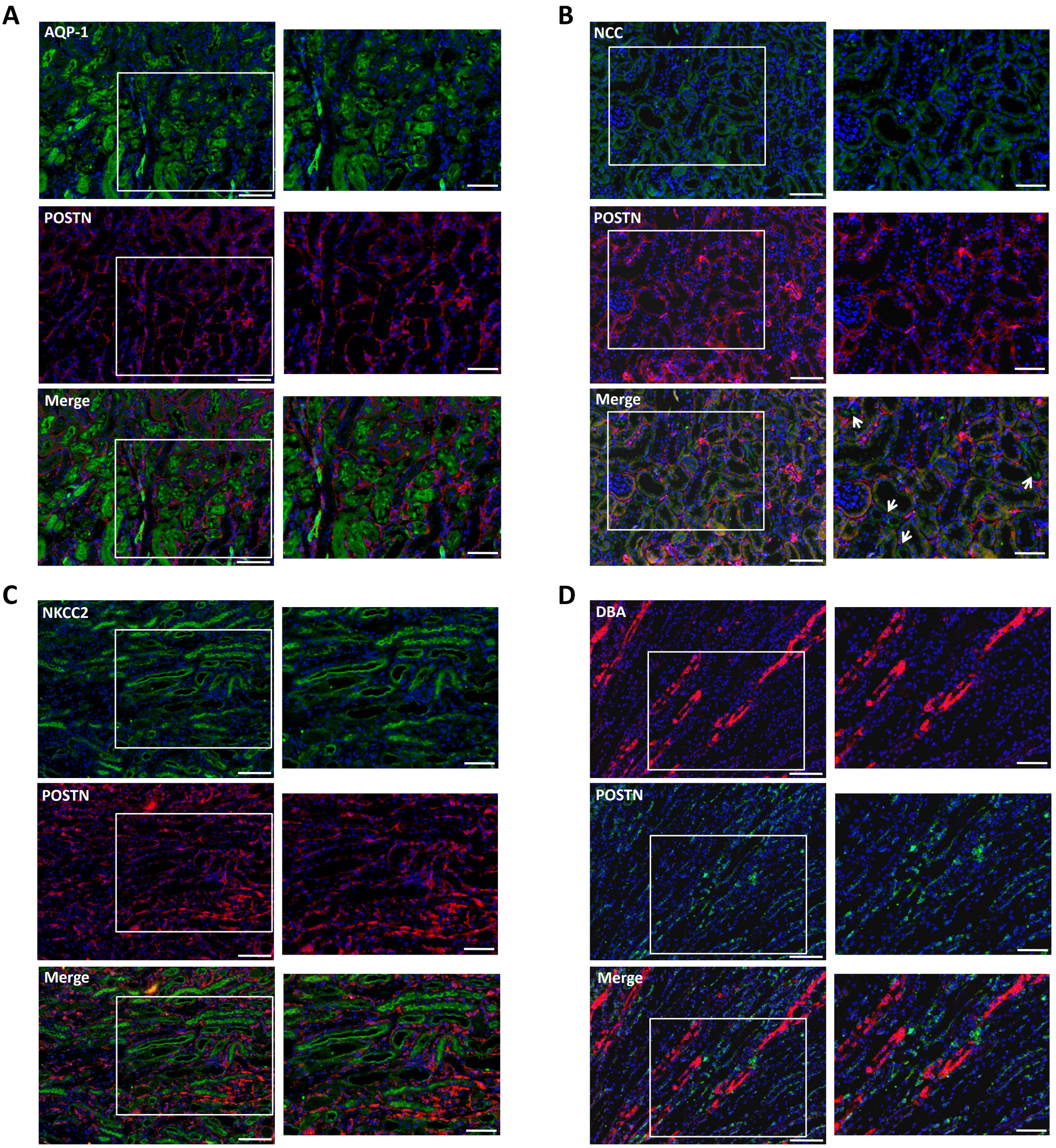

Supplemental Figure 2

A

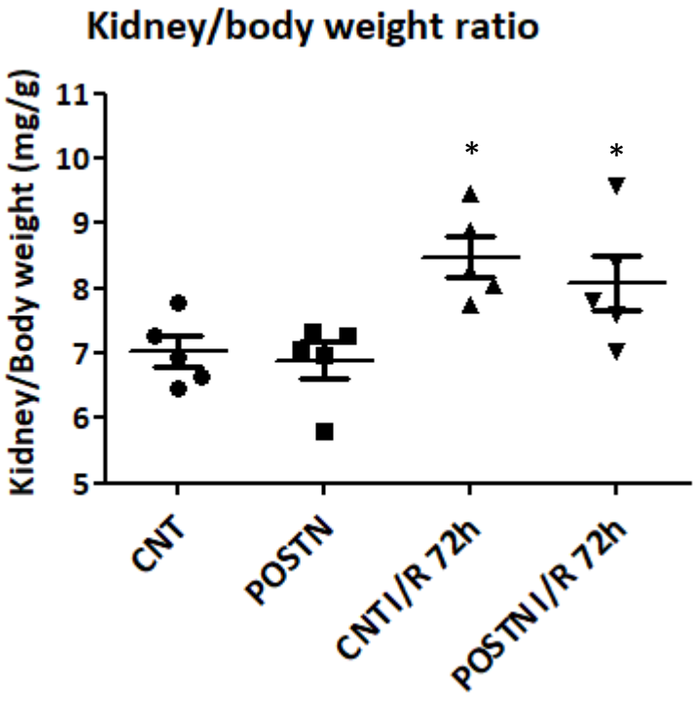

B

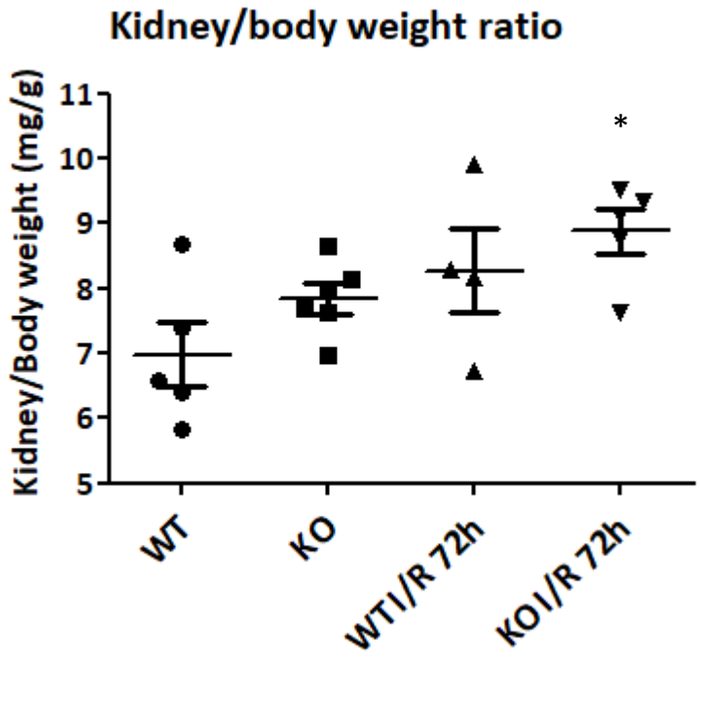

Supplemental Figure 3

A

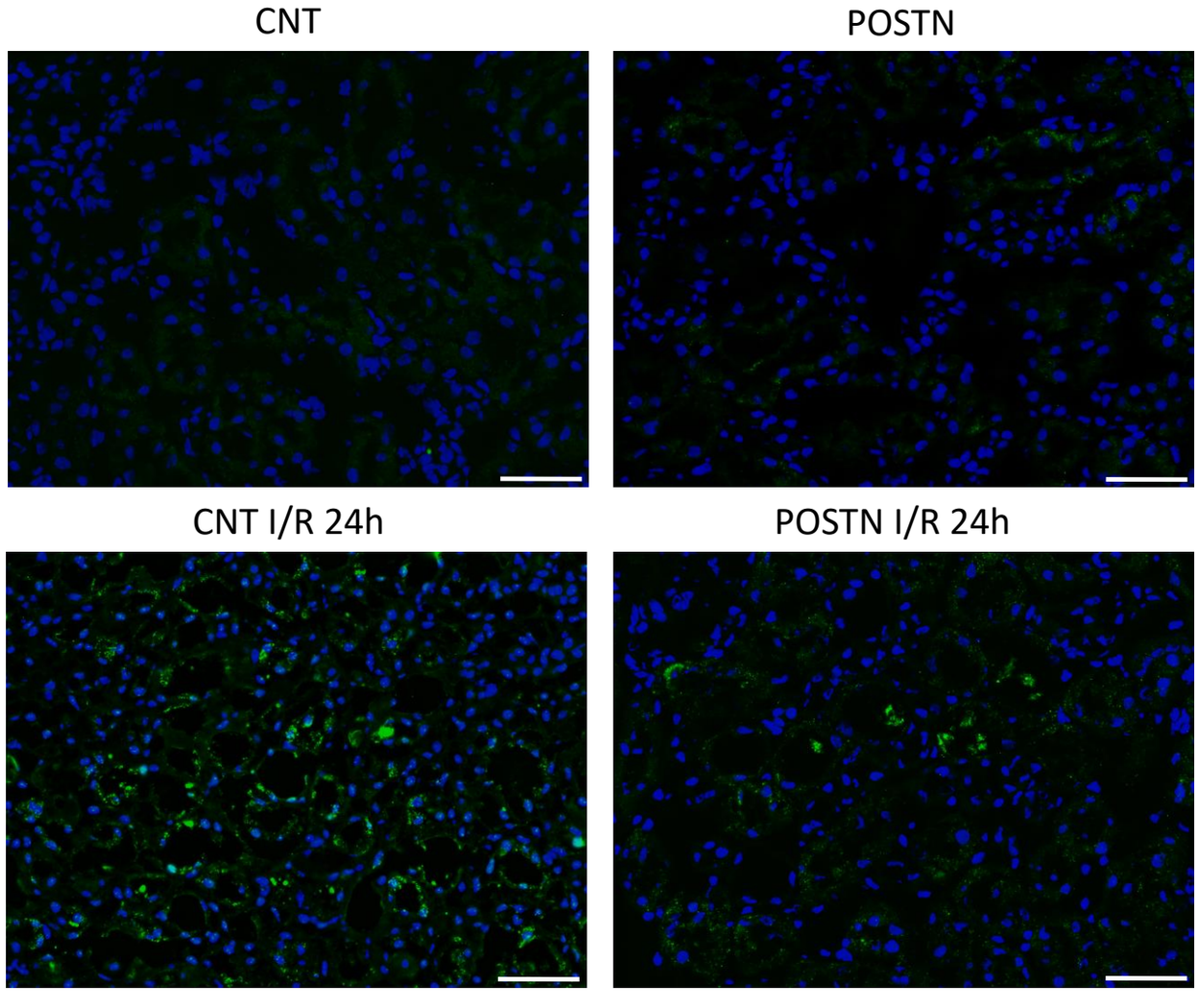

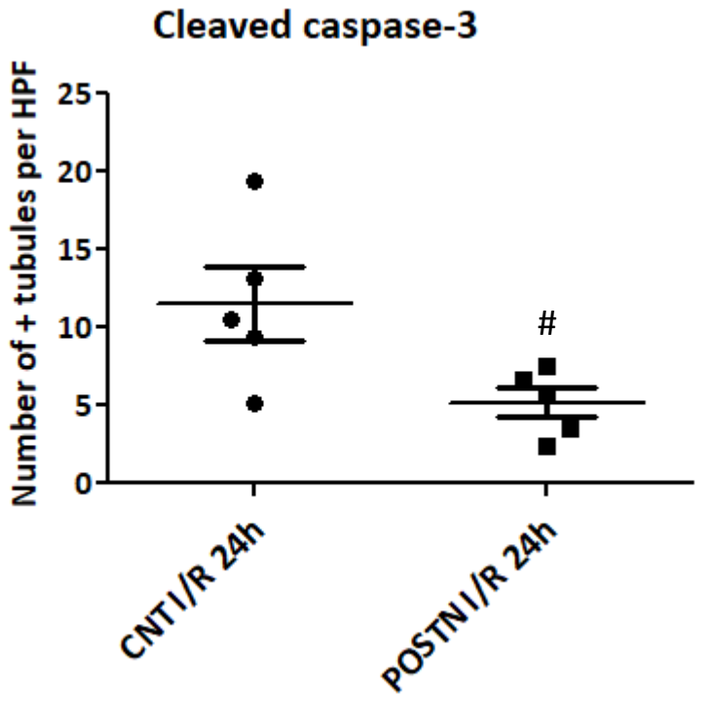

B

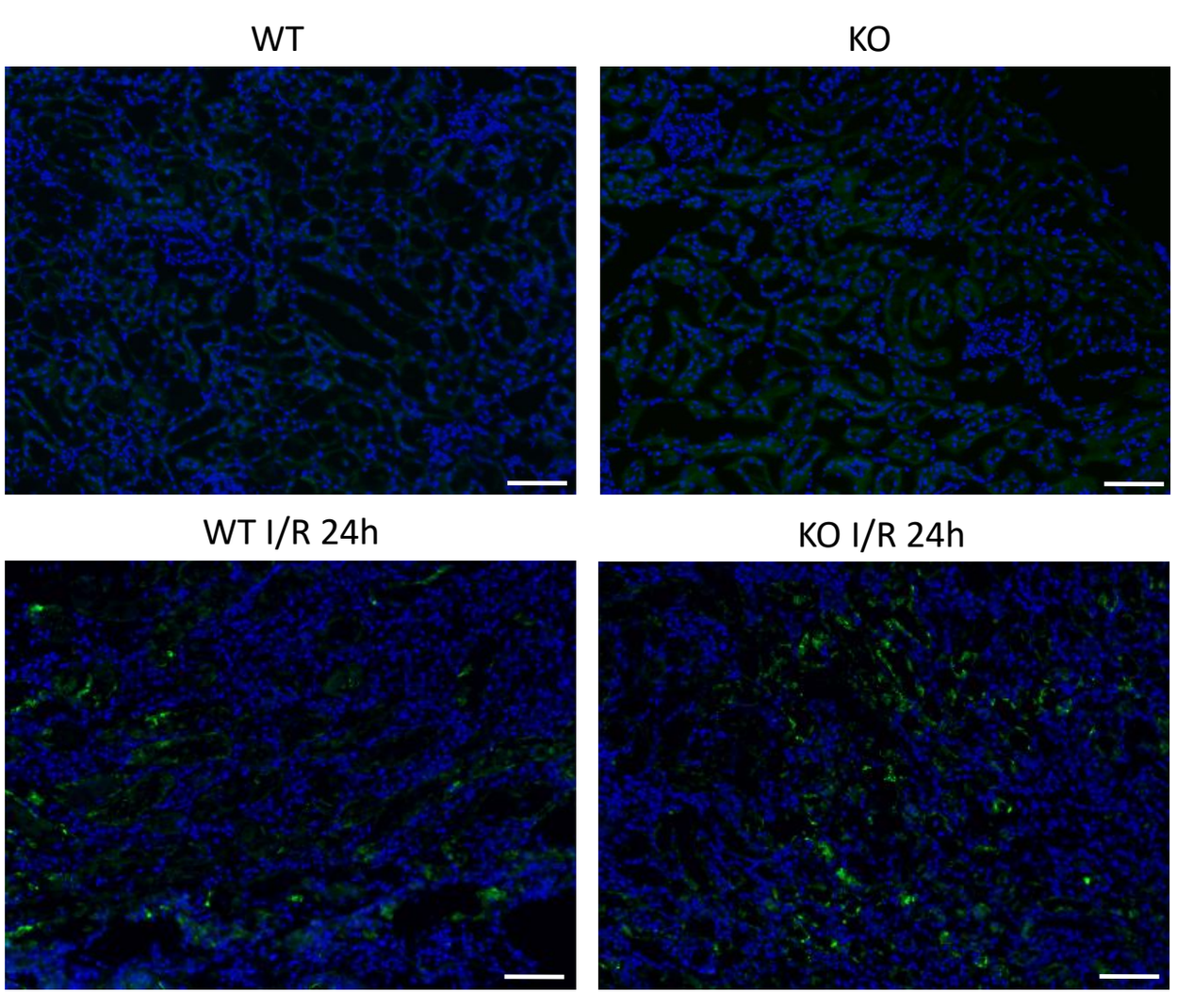

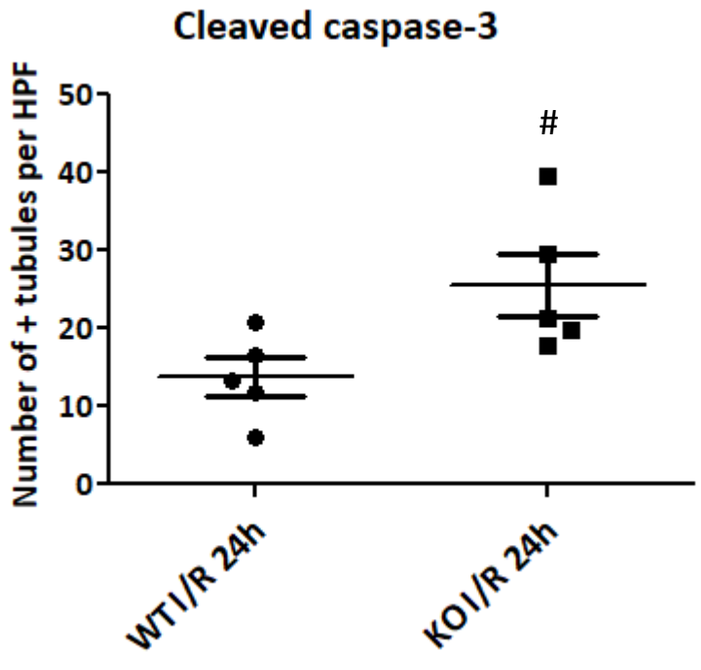

Supplemental Figure 4

A

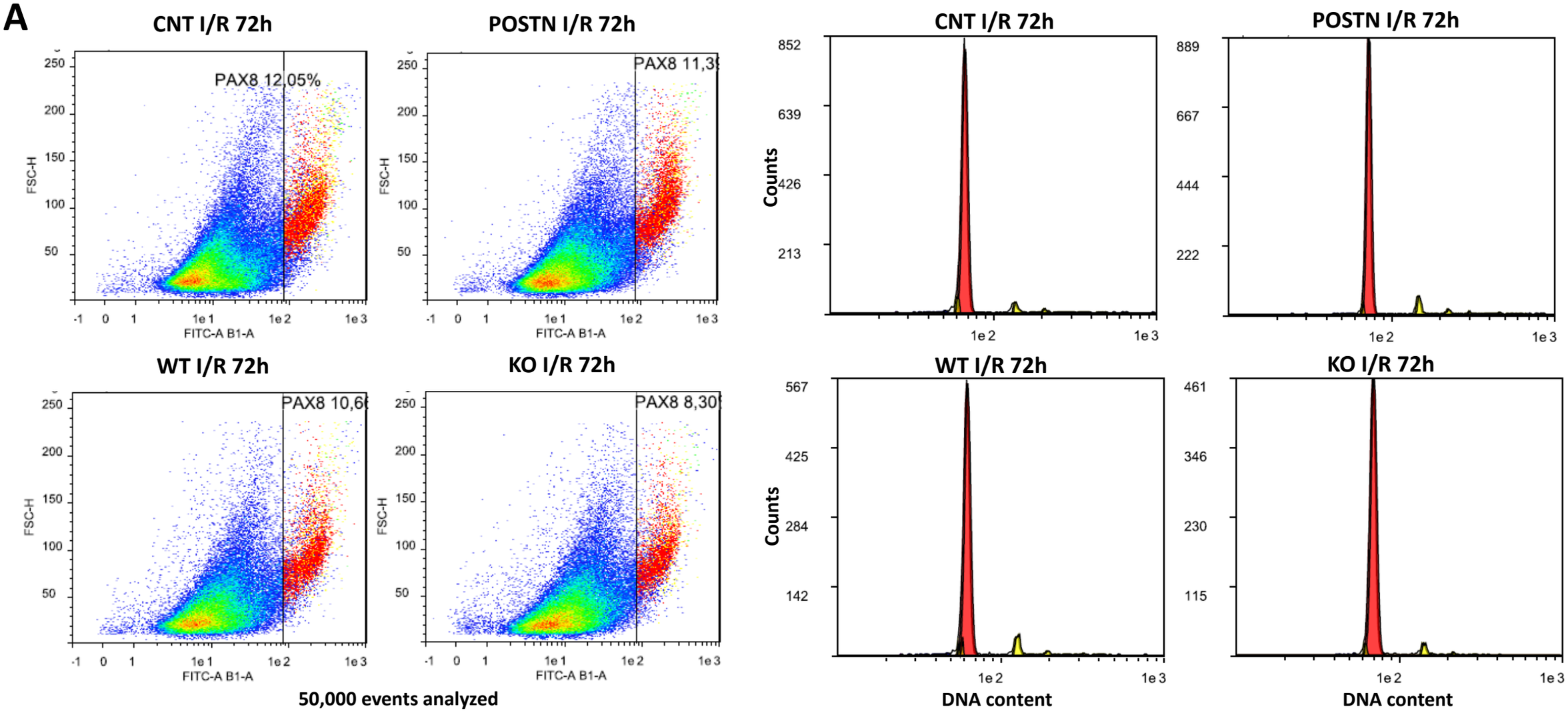

B

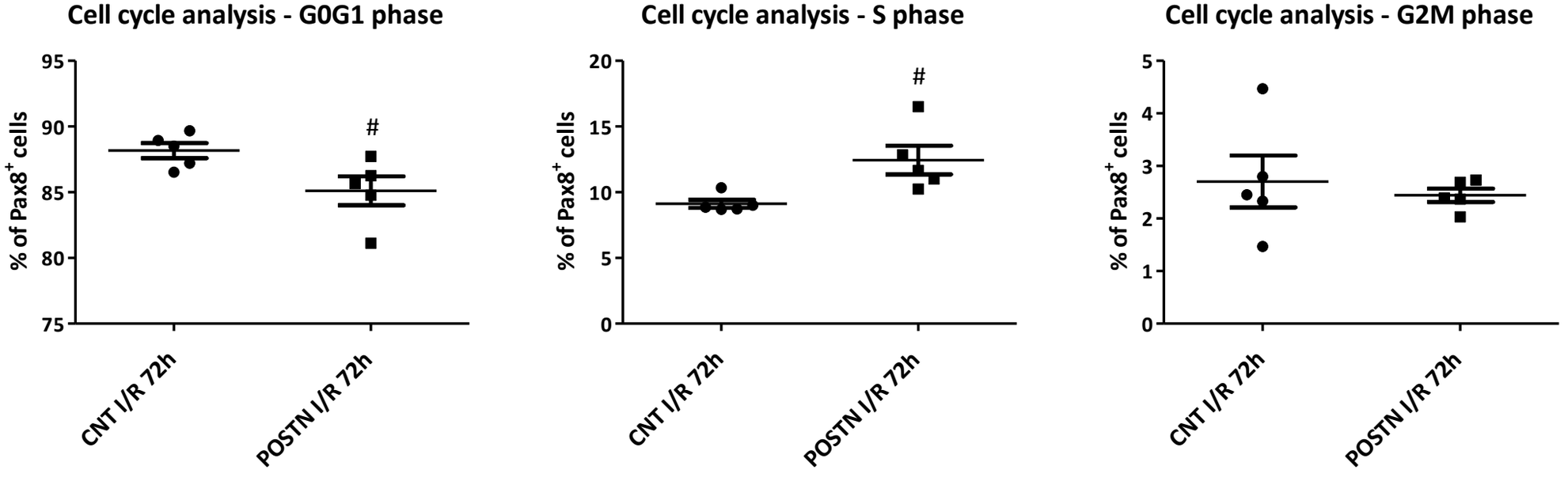

C

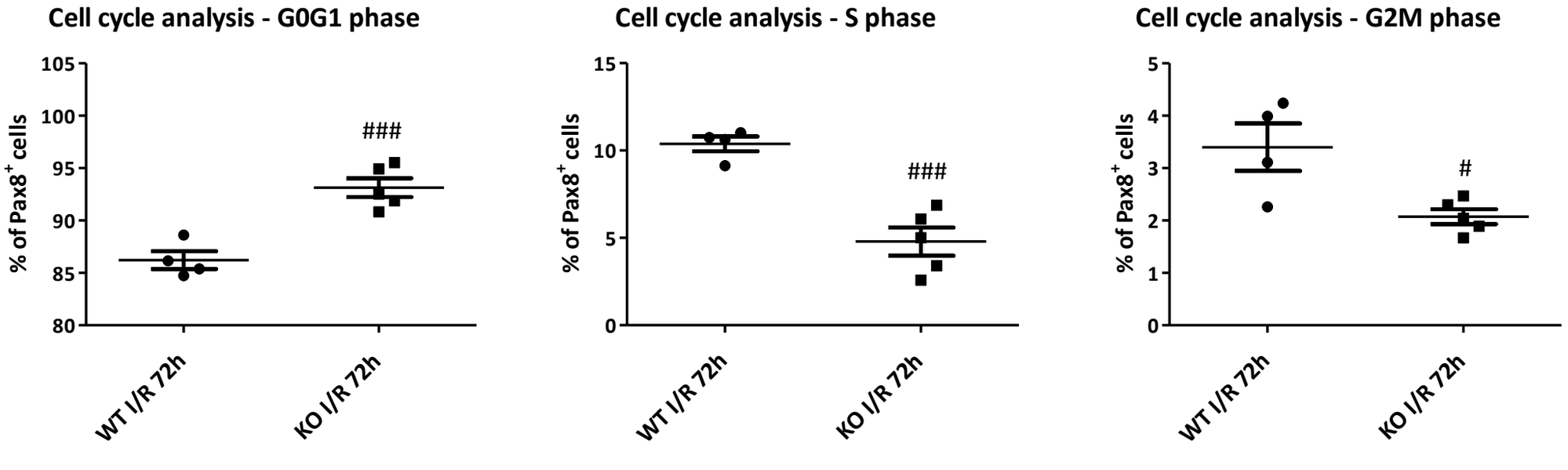

Supplemental Figure 5

A

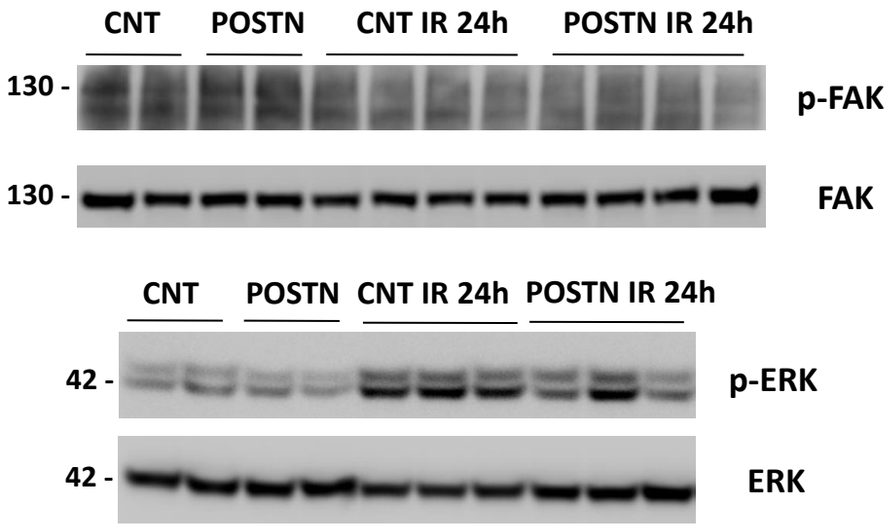

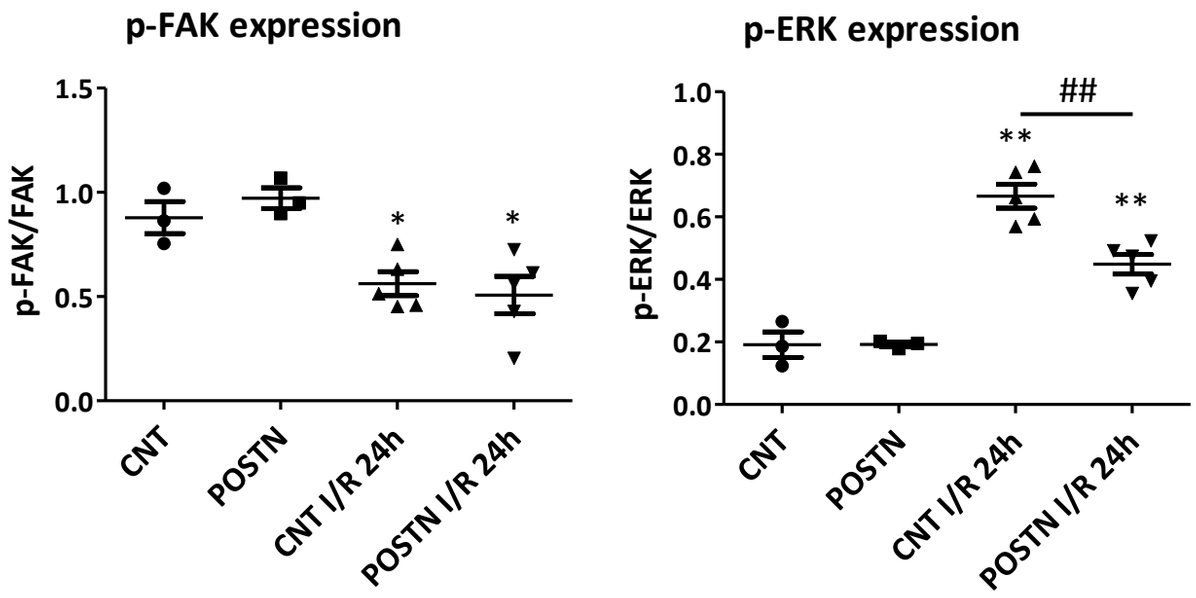

B

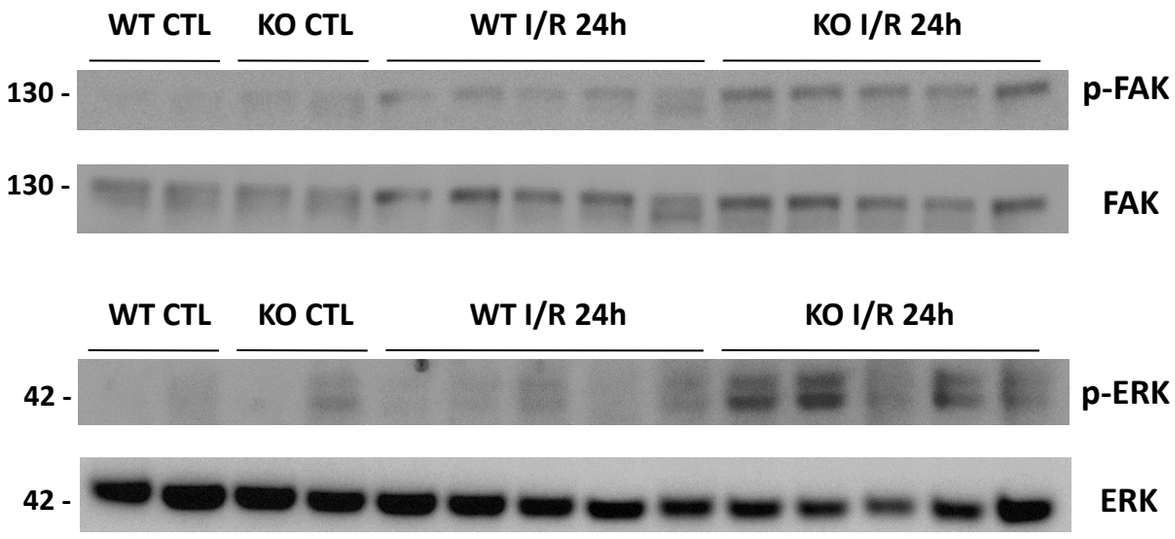

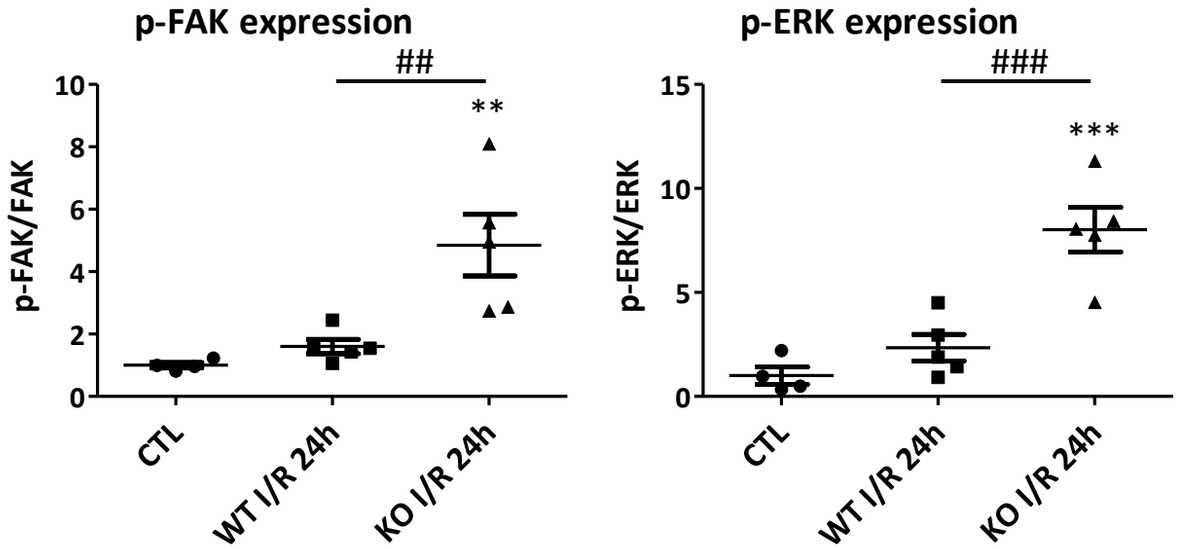

Supplemental Figure 6

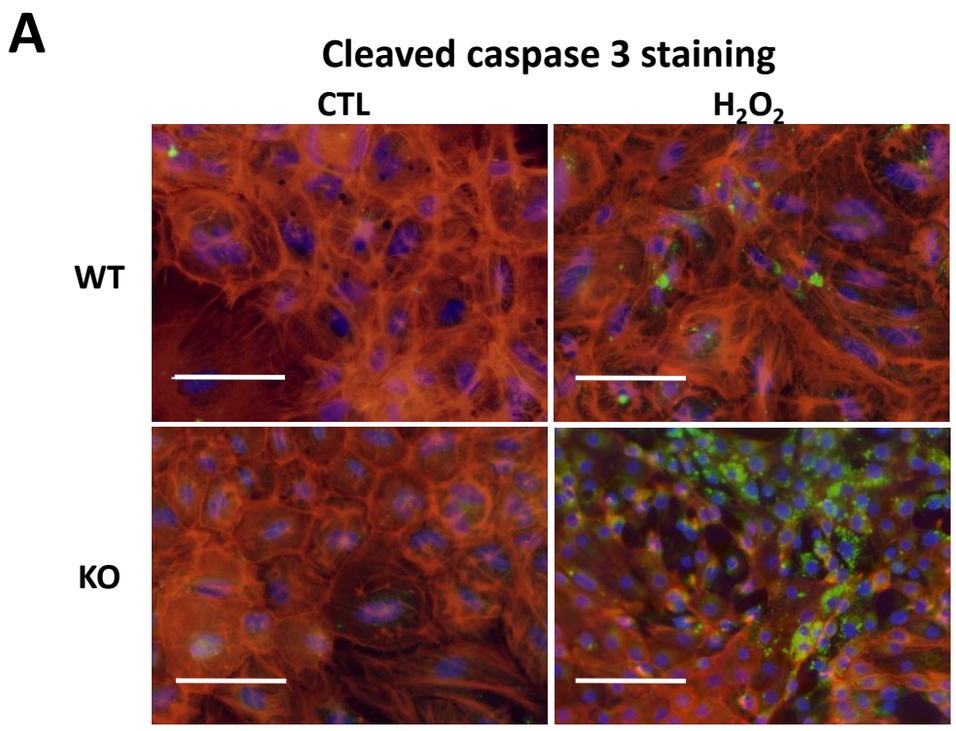

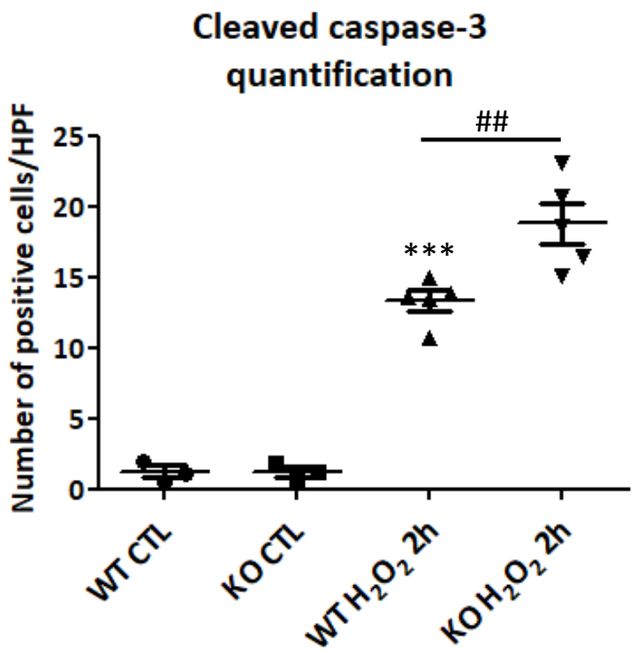

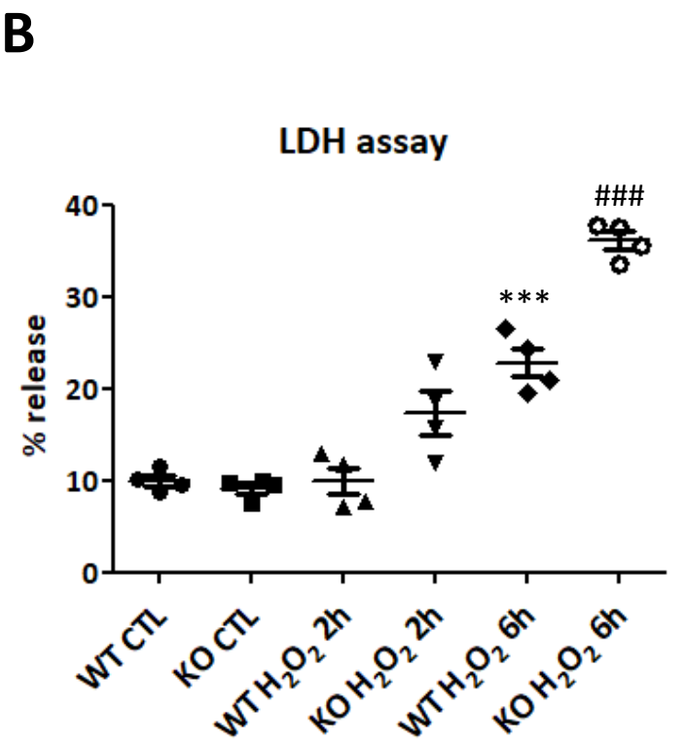

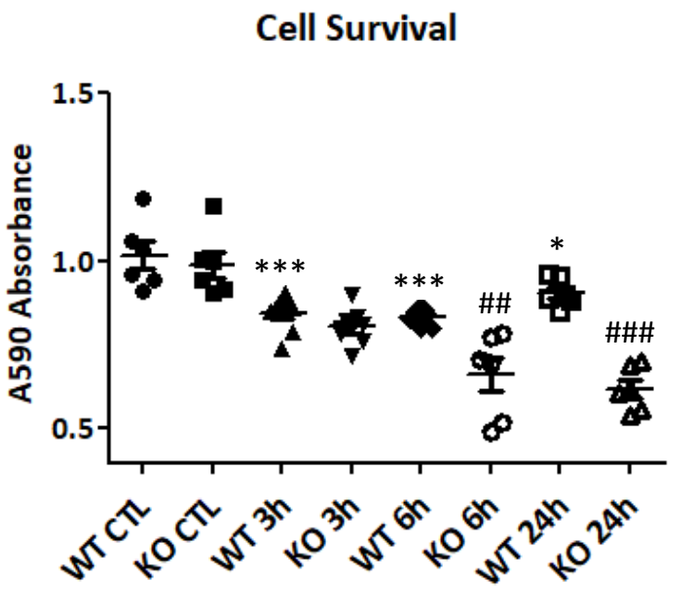

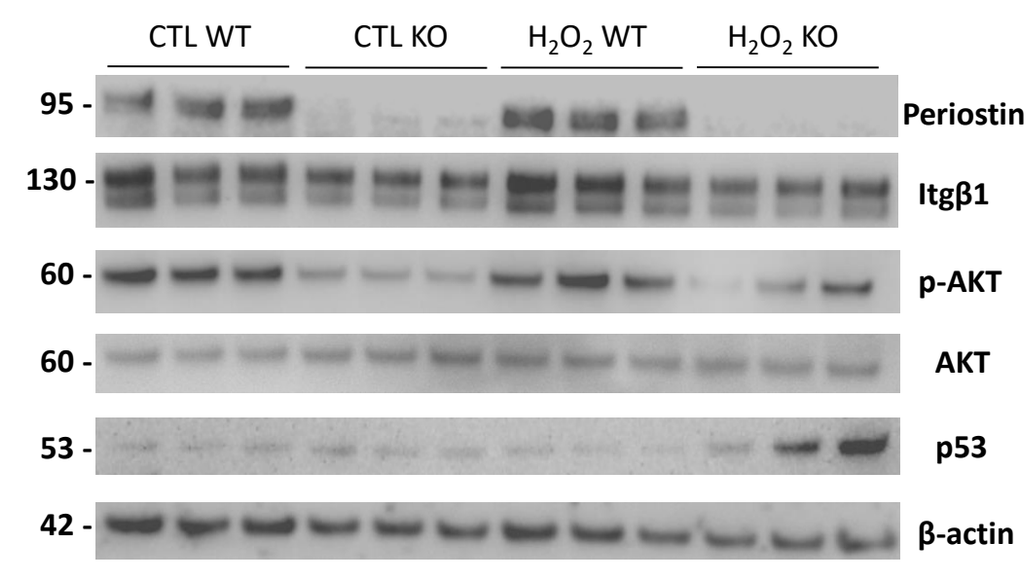

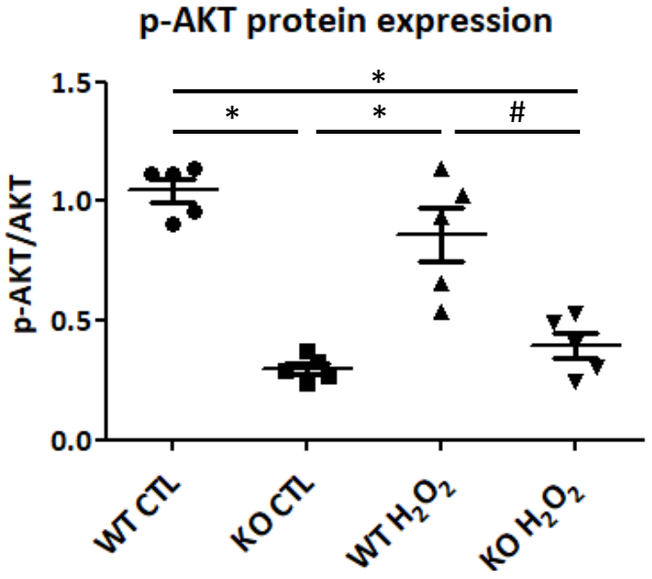

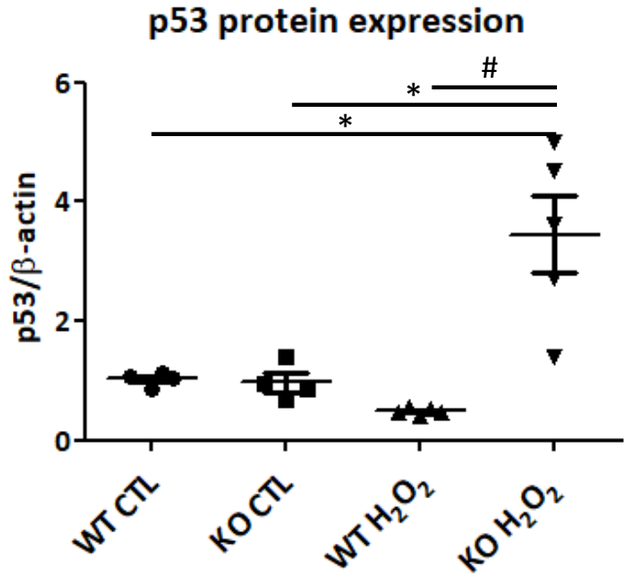

Supplemental Figure 7

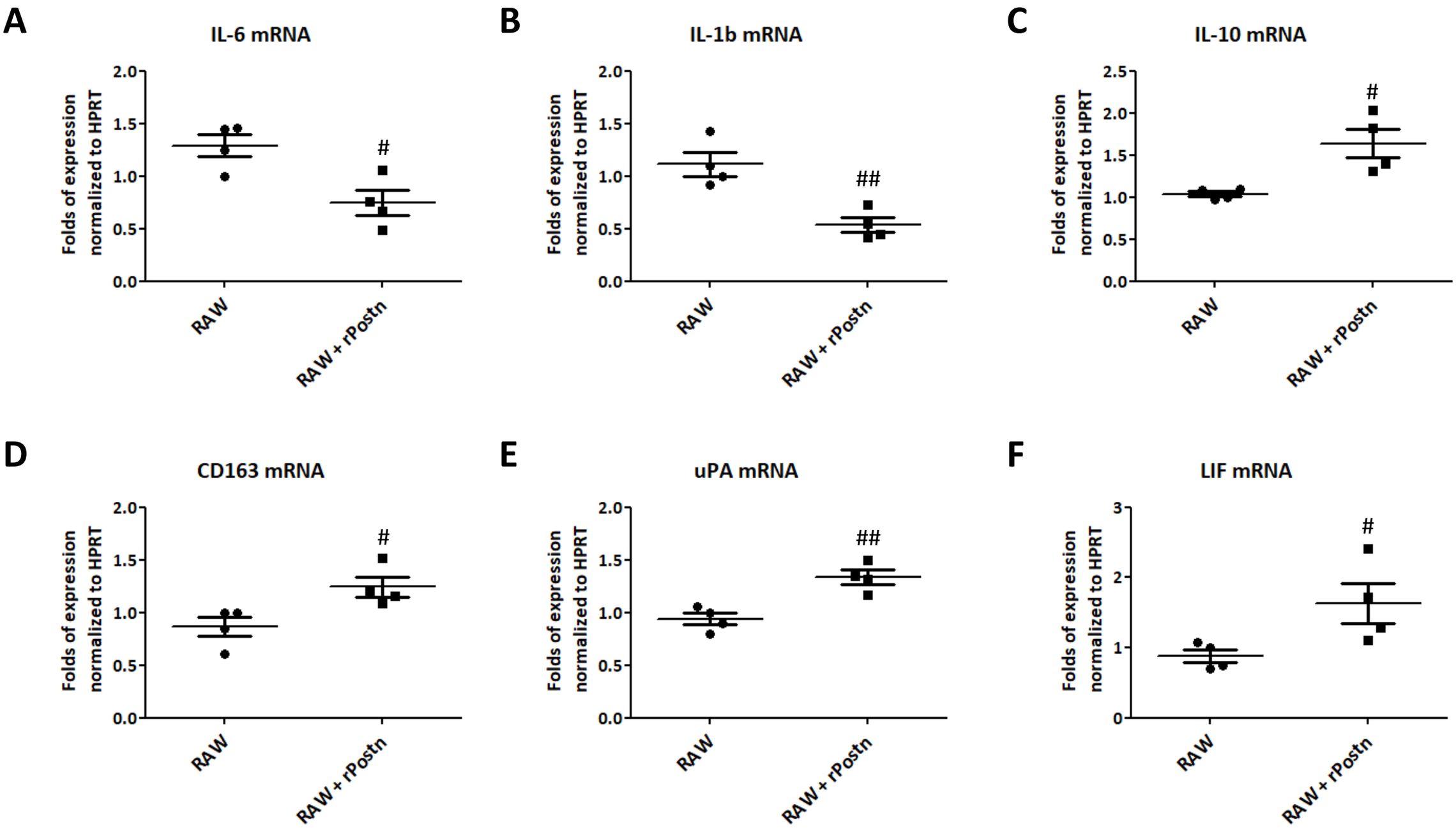

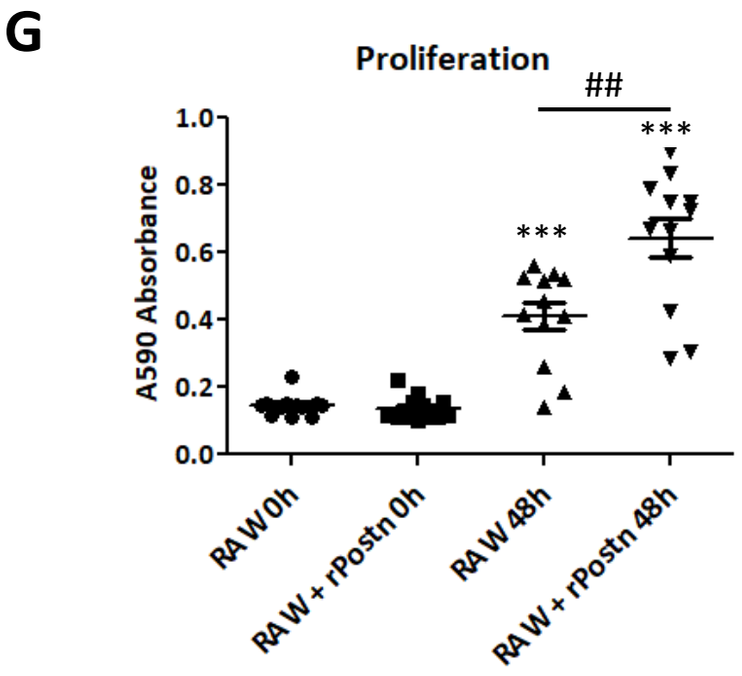

Supplemental Figure 8

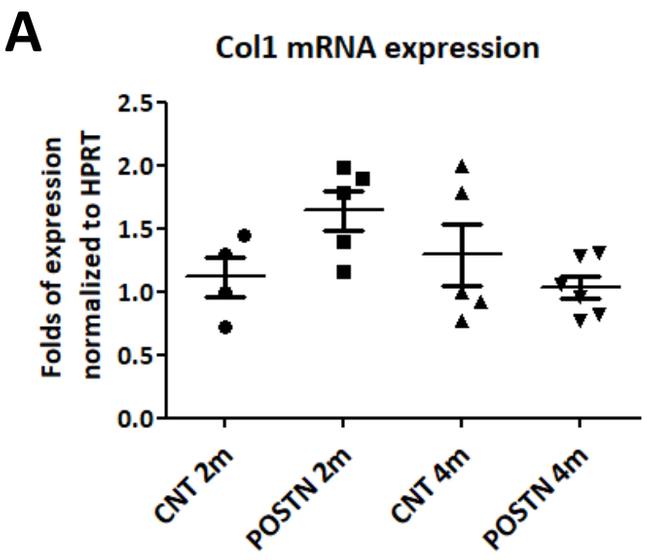

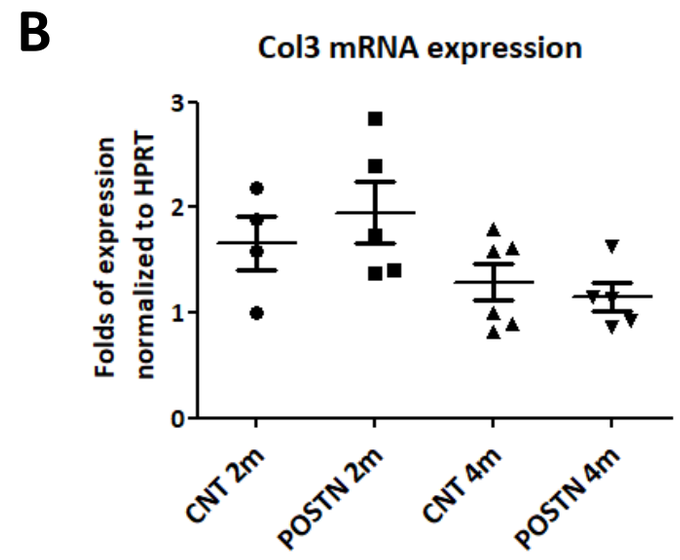

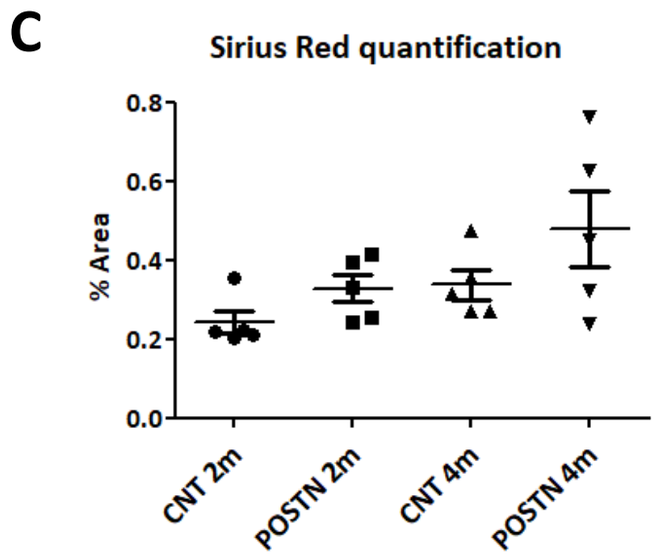

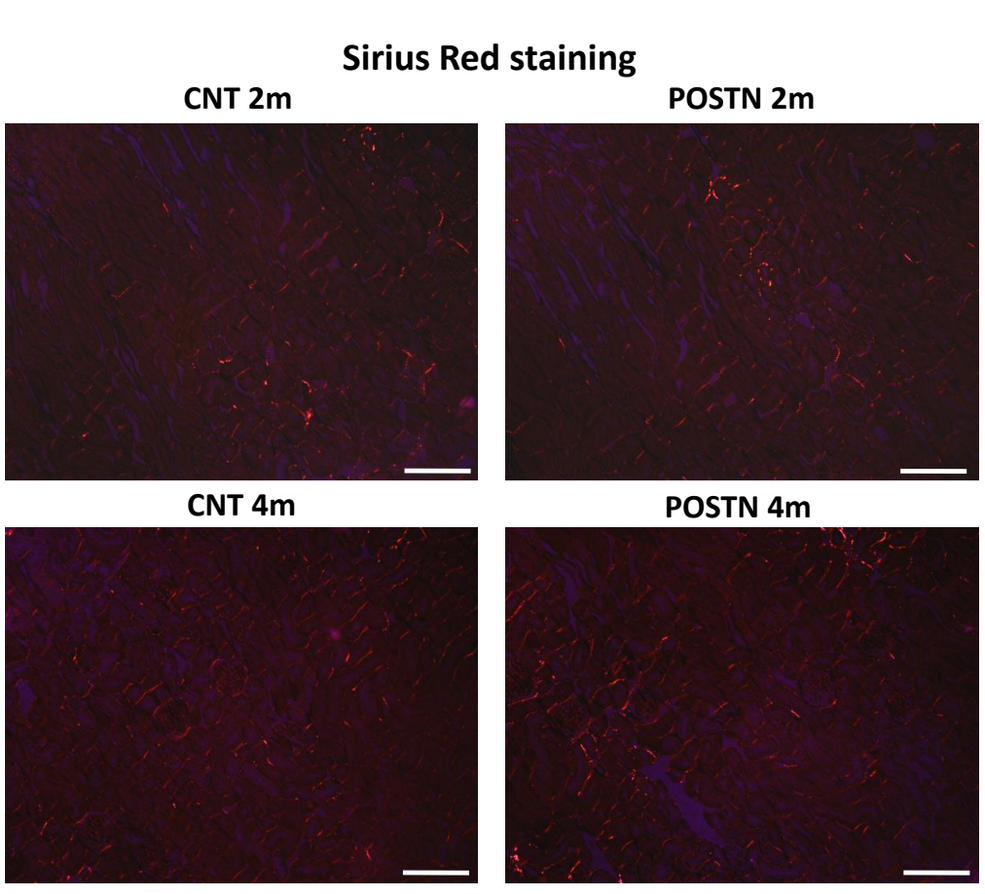

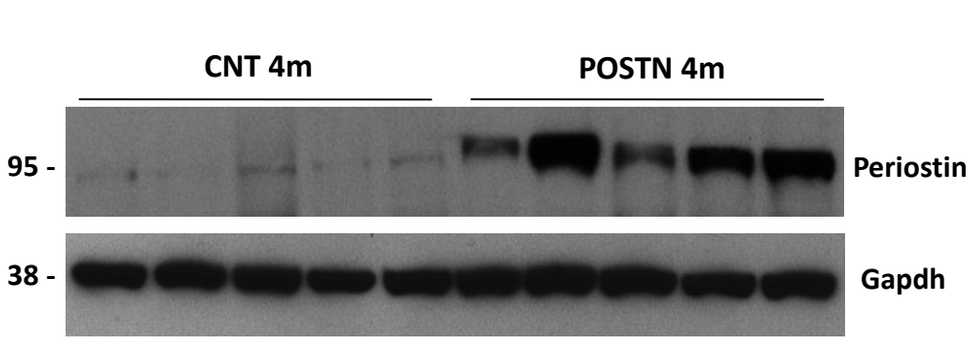

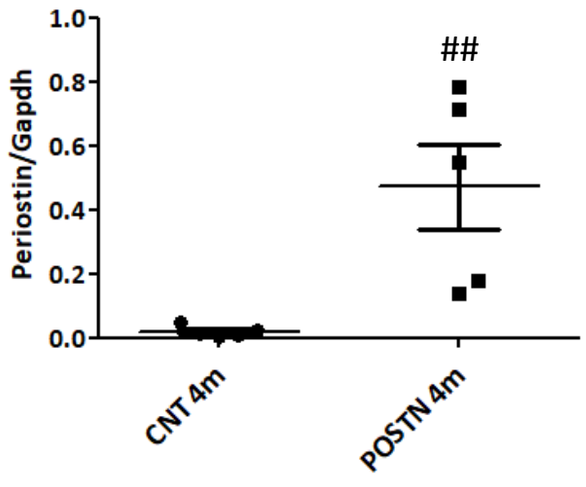

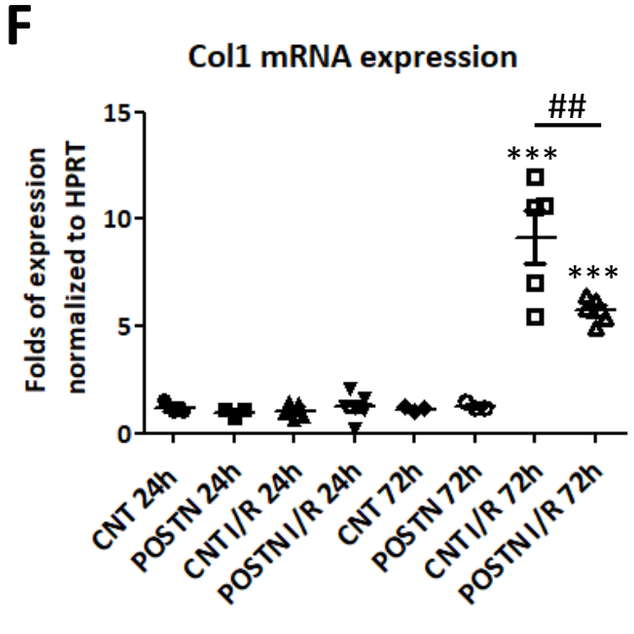

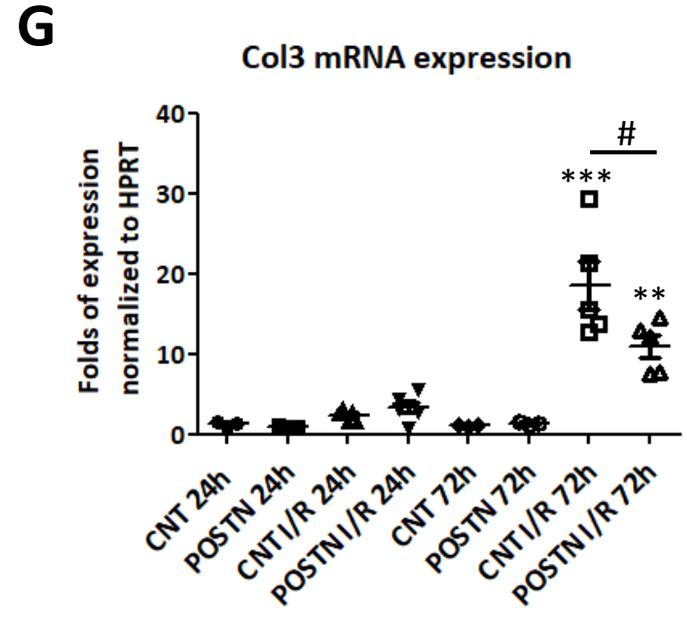

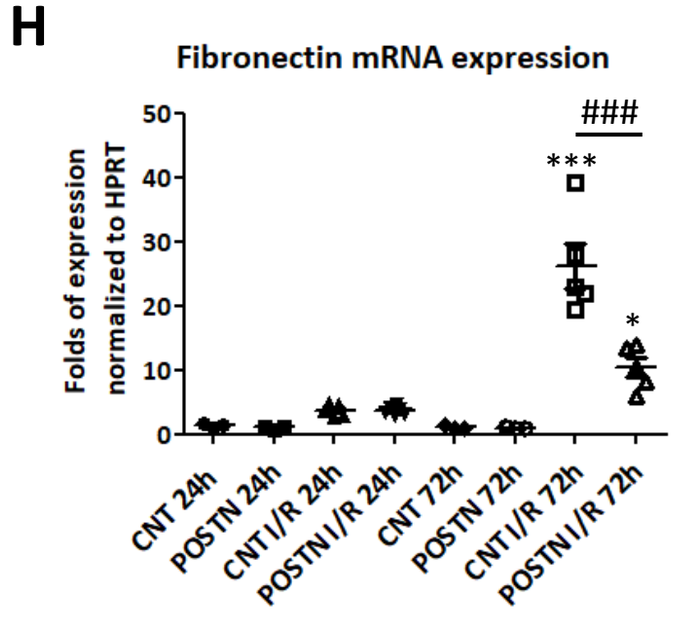

Supplemental Figure 9

A

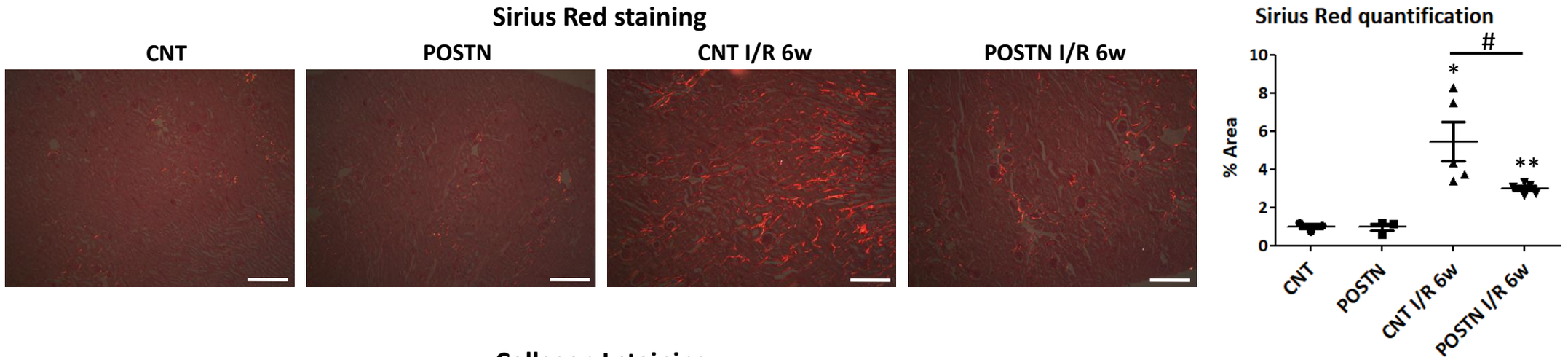

B

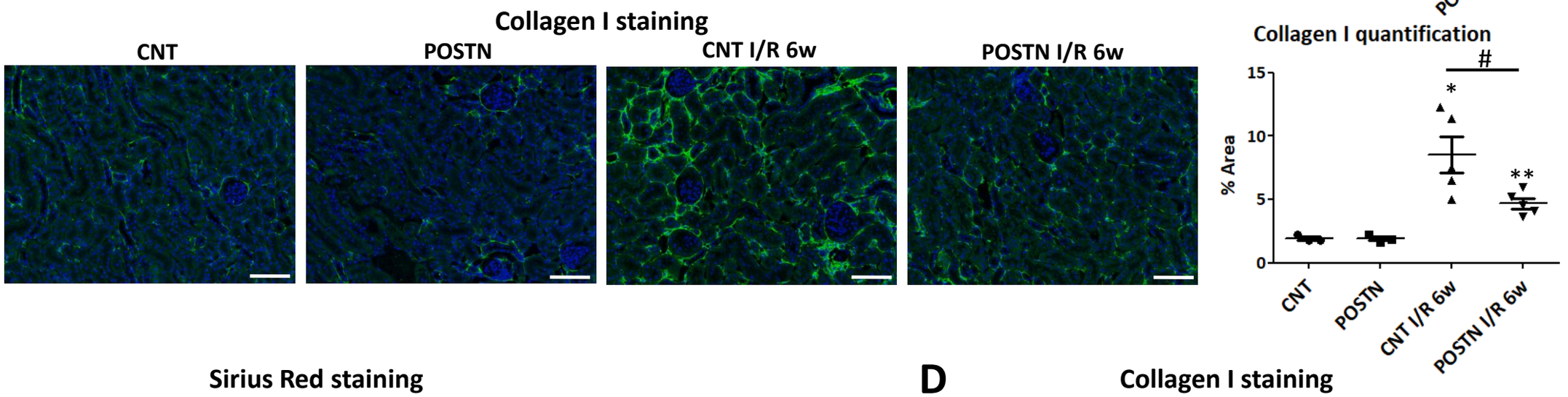

C

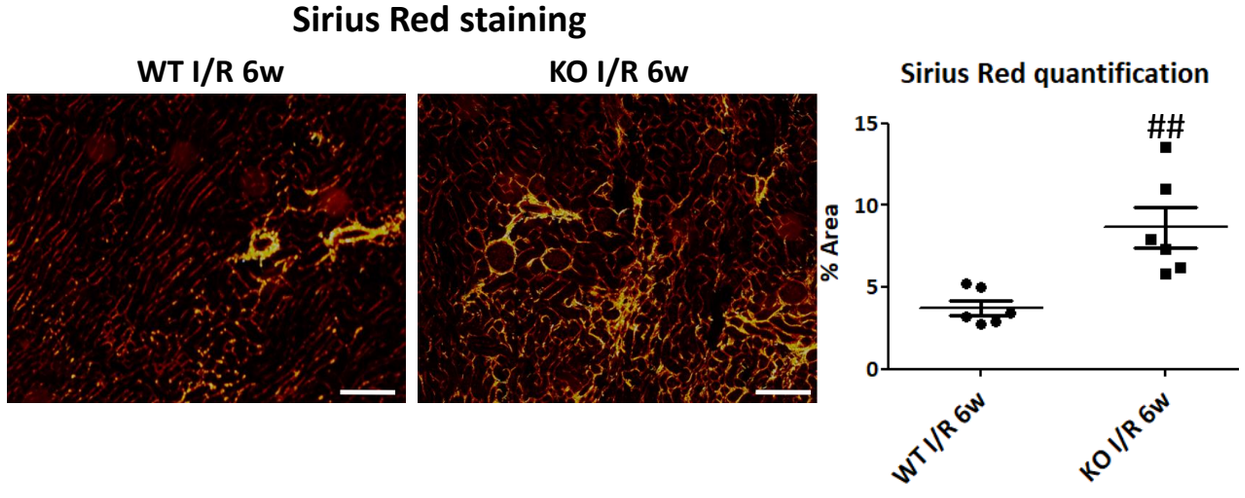

D

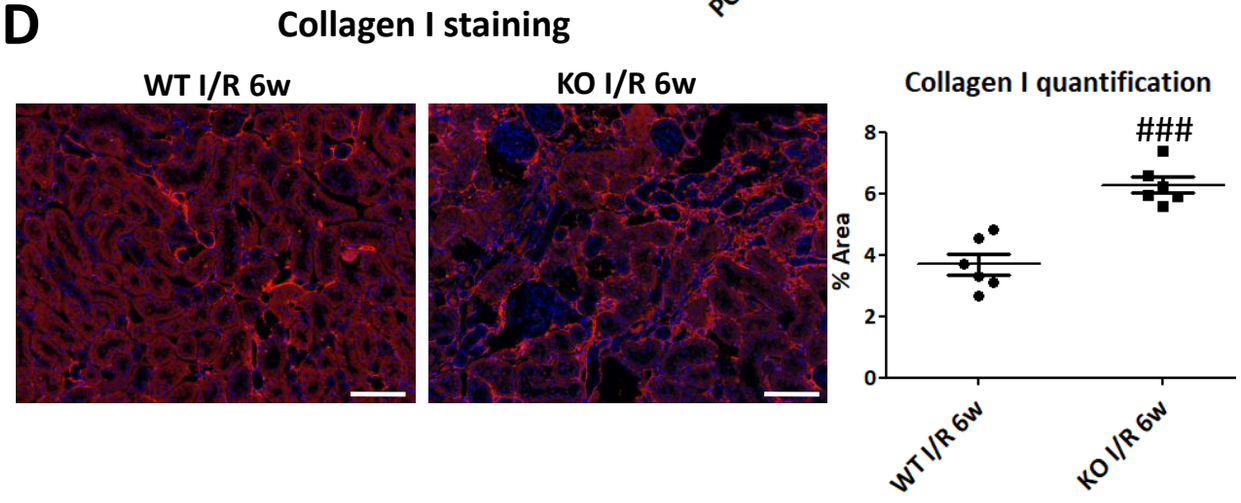

E

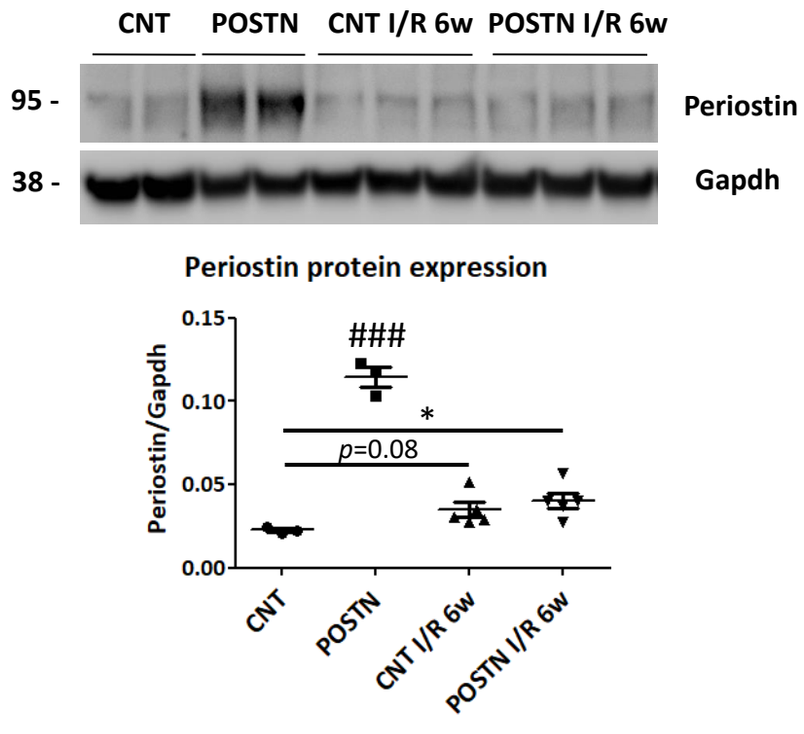

F

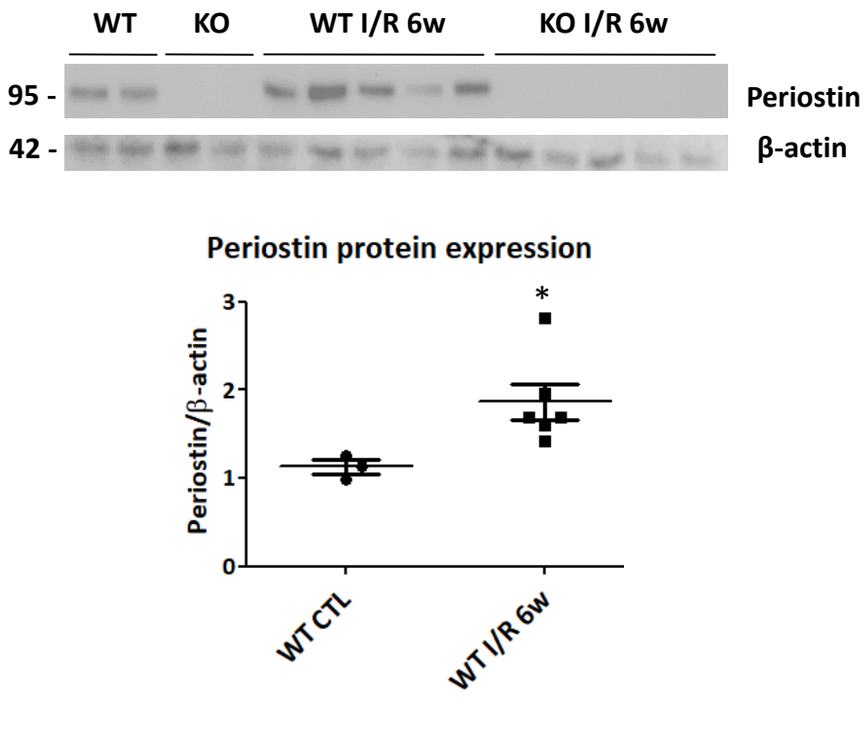

Supplemental Figure 10